Supporting Information

Regulation of DNA Repair Fidelity by Molecular Checkpoints: "Gates" in DNA Polymerase β's Substrate Selection

Ravi Radhakrishnan[‡], *Karunesh Arora*[§], *Yanli Wang*[¶], *William A. Beard*[⊥], *Samuel H. Wilson*[⊥] *and Tamar Schlick*[¶,*]

Appendix A: Study of R258A mutation in DNA polymerase β

Structural [1], kinetic [2], and computational data [3] have suggested that the large subdomain movement *per se* in the polymerase cycle is relatively rapid, while Arg258 side-chain rotation could be slow enough to be kinetically significant in the conformational change of pol β. Such slow rearrangements involving the Arg258 rotation might limit pol β's closing before chemistry. Transition path sampling simulations of pol β's correct incorporation also revealed that the transition state corresponding to Arg258 rotation is the rate-limiting step in the conformational change process [4]. Would these slow, local rearrangements surrounding Arg258 discourage incorrect nucleotide insertion? Would conformational barriers to closing be lower with Arg258 replaced by alanine? To address these questions, we study the R258A mutant enzyme using molecular dynamics and transition path sampling.

Methods

We construct the complex of pol β/DNA mutant R258A by replacing Arg258 with alanine in the wild-type intermediate model before chemistry [5], leaving other protein residues and DNA base sequences unchanged. The generated steric clashes in the mutant were removed by subsequent energy minimization and equilibration. The thumb subdomain in the initial R258A model was partially closed and the incoming nucleotide (dCTP) along with catalytic and nucleotide-binding magnesium ions were placed in the active site as in ternary crystal closed complex.

The intermediate R258A mutant model was solvated, minimized, and equilibrated as in our initial work [3, 5]. The mutant model contained about 40,000 atoms and was simulated over 15 ns with CHARMM.

In addition to this dynamics simulation, we employ the transition path sampling [6-8] approach as we developed for biomolecules [4, 9, 10]. As described in Ref. [4], trajectories in each transition state region were harvested using the shooting algorithm [6] to connect two metastable states via a Monte Carlo protocol in trajectory space. In each shooting run, the momentum perturbation size dP~0.002 in units of AMU×Å/fs was used to yield an acceptance rate of 25 to 30%.

For the free energy calculation [9], the probability distribution $P(\chi_i)$ was calculated by dividing the range of order parameter χ_i into 10 windows. The histograms for each window were collected by harvesting 300 trajectories per window according to the procedure in Ref. [9], from which the potential of mean force $\Lambda[\chi_i]$ was calculated. The arbitrary constant associated with each window was adjusted to make the Λ function continuous. The standard deviation in each window of the potential of mean force calculations was estimated by dividing the set of trajectories into two blocks and collecting separate histograms. The statistical error of $\pm 3k_BT$ in the free energy was estimated from the order parameter window showing the maximum standard deviation in the potential of mean force.

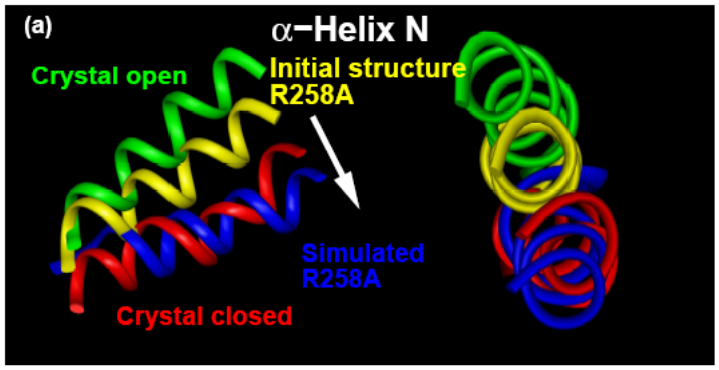

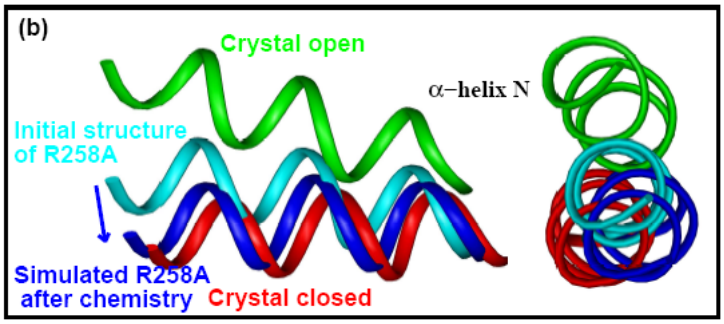

Figure S1: Comparison of α-helix N positions among crystallographic closed, open, simulated R258A, and R258A's initial reference structure, a) before chemistry, and b) after chemistry.

Results

Comparing the simulated R258A mutant structure with the crystallographic closed and open complexes (Fig. S1) using the position of α-helix N in the thumb subdomain, we observe that the R258A mutant with a correct dCTP incoming

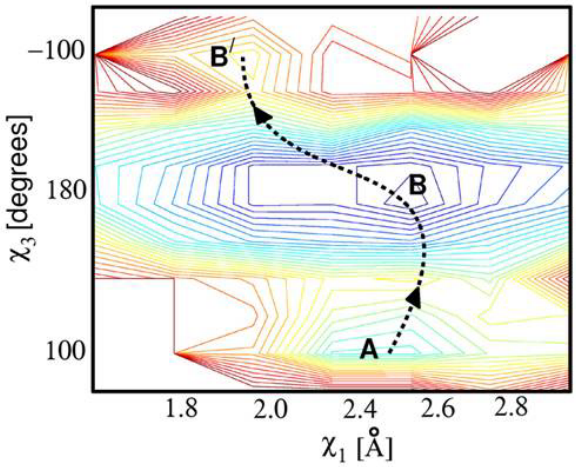

Figure S2: Contour plot of the two-dimensional histogram of χ_1 and χ_3 values visited in the harvested trajectories during the transition path sampling simulation corresponding to TS3 for the wild-type pol β.

nucleotide has approached a closed state.

In the transition path sampling study of the wide-type pol β complex, the relevant ranges of structural variables (χ_is) that define extent of sampling for each transition state (TS) are described by the lower and upper bounds χ_{min}, χ_{max} (see Ref. [4] for detailed definition). In particular, the variable (order parameter) employed to describe the thumb motion is χ_1, RMSD of heavy atoms in residues 275-295 of the thumb's α-helix N [11] in pol β with respect to the same atoms in the enzyme's closed state (1BPY); χ_1 varies from ~6 to ~1.5 Å, between the open and closed states. Another variable is χ_3, the dihedral angle of atoms C_γ-C_δ-N_ε-C_ζ and describes the rotation of Arg258 in wild-type pol β; χ_3 varies between ~100 and ~260° for open and closed states. A partially-rotated state of pol β (χ_3~180°) is also observed as a metastable state along the pathway for closing. Recall that our estimated free energy values along the closing pathway [4] suggested that the rate-limiting step is associated with transition state 3 (TS 3), i.e., the partial rotation of Arg258 (overall barrier of 20.5 ±3 k_BT). This value is lower but comparable to the overall rate of the reaction (25-28 k_BT), as obtained from experimental kinetic data k_{pol}, the overall rate of nucleotide incorporation of 1-10 s^{-1} [12-18].

We have previously reported that the RMSD deviation (χ_1) decreases from ~2.7 to 2.0 Å in crossing TS 3. This concomitant motion of thumb with the rotation of Arg258 in wild-type pol β is revealed by a two-dimensional contour plot of χ_3 and χ_1 visited in the dynamics trajectories during the transition path sampling calculation (Fig. S2).

To probe the effect of the R258A mutation on the free energy landscape associated with

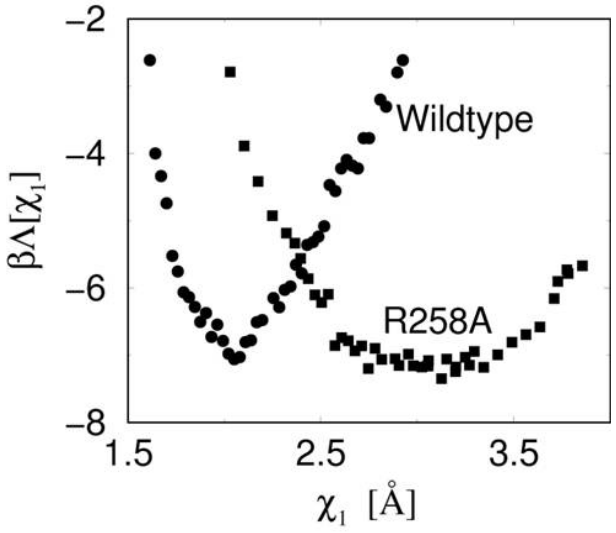

Figure S3: Potential of mean force along χ_1 corresponding to transition state 3 for wild-type and R258A mutant enzymes.

TS 3, we compute the potential of mean force associated with the mutant enzyme corresponding to this transition state. Because the order parameter χ_3 characterizing the rotation of Arg258 no longer exists for the mutant enzyme, but the evolution of χ_1 is related to that of χ_3 for the wild-type enzyme (Fig. S2), we compare the potential of mean force along χ_1 for the wild-type and mutant enzymes (Fig. S3).

The free energy landscape corresponding to TS 3 for the wild-type enzyme is characterized by a barrier for rotation of 13 k_BT for Arg258 [10]. The concomitant closing of the thumb provides thermodynamic stabilization for the system, as the potential of mean force is decreasing in the range $2.7 < \chi_1 < 2.0$ Å. In contrast, for the R258A system, because of the alanine substitution the landscape along χ_1 is flat in the range $3.4 < \chi_1 < 2.6$ Å. Taken together, these results point to a barrier-less TS 3 for the mutant enzyme, in sharp contrast to the wild-type enzyme. If we make the additional assumption that the R258A mutation does not impact the energy landscape associated with the rest of the transition states (TS 1, 2, & 4) considerably, we can make the following deductions about the closing kinetic pathway for the mutant enzyme. A barrier-less TS 3 for R258A implies that TS 1 (thumb closing) is rate-limiting in the closing pathway. The rate of conformational closing for wild-type is given by $(1/\tau)\times\exp[-\beta\{F(TS3)- F(open)\}]$ and that for the R258A mutant is given by $(1/\tau)\times\exp[-\beta\{F(TS1)- F(open)\}]$. Here, τ is the time-scale for crossing the transition state and F is the Helmholtz free energy. (Estimates for τ and F are available in Refs. [4, 10].) Using the calculated values of F and τ (see Ref. [4]) , we employ a stochastic reaction network model (as done in [10] for the wild-type) to calculate time evolution of the conformational closing transition for the mutant in comparison to that of the wild-type. The model is summarized below:

Wild-type: $Open(A) \underset{k_{-1}}{\overset{k_1}{\Leftrightarrow}} B \underset{k_{-2}}{\overset{k_2}{\Leftrightarrow}} C \underset{k_{-3}}{\overset{k_3}{\Leftrightarrow}} D \underset{k_{-4}}{\overset{k_4}{\Leftrightarrow}} E \underset{k_{-5}}{\overset{k_5}{\Leftrightarrow}} F(Closed) \underset{k_{-7}}{\overset{k_7}{\Leftrightarrow}} Product(G)$

R258A: $Open(A) \underset{k_{-1}}{\overset{k_1}{\Leftrightarrow}} B \underset{k_{-2}}{\overset{k_2}{\Leftrightarrow}} C \underset{k_{-4}}{\overset{k_4}{\Leftrightarrow}} E \underset{k_{-5}}{\overset{k_5}{\Leftrightarrow}} F(Closed) \underset{k_{-7}}{\overset{k_7}{\Leftrightarrow}} Product(G)$

The rate-constants for the network model (in s^{-1}) calculated from our free energy simulations were found to be [4, 10]: (a) for wild-type, k_1=12000, $k_{-1}=1\times10^8$, $k_2=5\times10^9$, $k_{-2}=6\times10^8$, $k_3=2\times10^7$, $k_{-3}=1\times10^4$, $k_4=5\times10^9$, $k_{-4}=6\times10^8$, $k_5=2\times10^9$, $k_{-5}=3\times10^7$, k_6=10, k_{-6}=0, and (b) for R258A mutant, k_1=12000, $k_{-1}=5\times10^6$, $k_2=5\times10^9$, $k_{-2}=6\times10^8$, $k_4=5\times10^9$, $k_{-4}=6\times10^8$, $k_5=2\times10^9$, $k_{-5}=3\times10^7$, k_6=10, k_{-6}=0. The stochastic time evolution for the closed state (F) and the product (G) for wild-type and R258A mutant is shown in Figure S4.

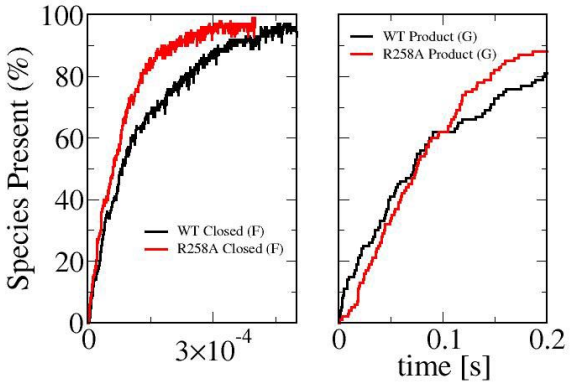

Figure S4: Time evolution of species (closed state and product) according to the reaction network model for wild-type (WT) mutant and R258A.

The barrier-less transition state 3 (for R258A) translates to a speedup of the conformational closing by a factor of 2 (time to reach 66% of maximum value of the closed state is 1.8×10^{-4} s for wild-type versus 8×10^{-5} s for R258A, see Fig. S4). This in-turn translates to a speedup of the overall incorporation step or k_{pol} (conformational closing plus chemistry) by a factor of 1.3 (time to reach 66% of maximum value of the product state is 0.13 s for wild-type, and 0.10 s for R258A, see Fig. S4). Experimentally measured k_{pol} for R258A is a factor 2-4 fold greater than the wild-type (Beard et al., unpublished results). Therefore, our results are in good agreement with experimental data.

Discussion

Our dynamics simulation for the R258A mutant indicates that the thumb moves toward a ‘closed’ state, similar to the crystallographic closed structure [11]. Thus, the subtle residue changes in the vicinity of the polymerase active site affect the subdomain motion and may indicate that the equilibrium constant for this structural transition is near unity. This is quantitatively verified by the free energy changes we have delineated for the wild-type pol β closing before chemistry, where find that the free energy difference between the open and closed states for the correct nucleotide at the active site is zero within the error bars of our calculation.

Since Asp192 forms a salt-bridge with Arg258 in the open inactive conformation while it coordinates both the catalytic and nucleotide-binding Mg^{2+} in the closed active conformation, removing the positive charge on residue 258 would be expected to promote the active closed conformation because Asp192 would be free to coordinate both Mg^{2+} ions required for catalysis. Indeed, we note a favored closed conformation for the simulated R258A. Our free energy calculation for the transition state corresponding to Arg258 rotation in the R258A mutant clearly indicates a barrier-less landscape which supports the enhanced rate of conformational closing for R258A.

A facilitated closing in R258A agrees with its increased rate of nucleotide insertion (Beard et al., unpublished observation) relative to the wild-type enzyme. The single-residue mutation in the active site may alter the enzyme's conformational closing and/or affect the chemistry step (if rate-limiting), and thus change the rate of nucleotide insertion, k_{pol}.

This behavior is borne out in the results of our reaction network model. A summary of dynamics trajectories and the free energy landscape from this work and Refs. [3-5, 10, 19, 20] is sketched in Figure S5. For wild-type pol β, consistent with our delineated free energy landscape for the conformational closing pre-chemistry [4, 10], dynamics trajectories initiated from an intermediate configuration of the ternary complex with a correct nucleotide evolve towards and reach a closed conformation of the complex (Fig. S5, top left, black arrow). This validates our finding that the closed ternary complex of a correct base-pair at the active site is thermodynamically more stable than the open conformation. The dynamics trajectory initiated from the same intermediate complex without the incoming nucleotide

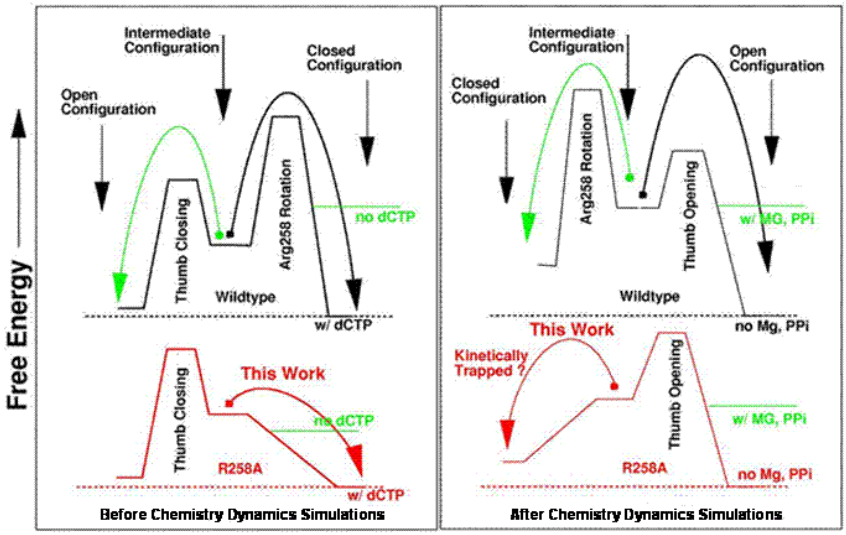

Figure S5: Summary of dynamics trajectories and the free energy landscape for R258A and wild-type pol β.

evolves towards and reaches an open conformation. This suggests that the incoming nucleotide is necessary for the stabilization of the closed state (Fig. S5, top left, green arrow). Our dynamics trajectory of a ternary complex of an R258A mutant initiated from the intermediate complex with a correct base pair at the active site also evolves towards the closed state (Fig. S5, bottom left, red arrow). However, the timescale for the R258A trajectory to reach the closed state is much shorter in comparison with the wild-type case. This observation is consistent with our finding of a barrier-less TS 3 due to the alanine substitution at 258 (see Fig. S3).

Our dynamics trajectories for the wild-type pol β after chemistry (see [21]) support a scenario in which the free energy landscape post chemistry is symmetric with respect to that of closing pre-chemistry. In particular, trajectories initiated from an intermediate state (with the Mg^{2+} and PP_i groups still associated with the active site) evolve toward the closed state, while the removal of Mg^{2+} and PP_i leads trajectories toward the open state (Fig. S5, top right). The analogous trajectory for the R258A mutant system with no Mg^{2+} and PP_i in the active site, however, evolves towards the closed state, possibly indicating a kinetically trapped conformation (Fig. S5, bottom right, red arrow).

The free energy landscape for conformational closing before chemistry for an incorrect nucleotide at the active site reveals that the Arg258 rotation step is no longer rate-limiting this system [10]. Consistent with this result, it is experimentally observed that R258A does not have a significantly altered fidelity with respect to the wild-type enzyme (Beard et al., unpublished observation). This may however also imply that both correct and incorrect insertions are likely influenced similarly by the alanine substitution. Simulations of a mutant system with a mismatch in the active site are needed to validate this hypothesis.

Appendix B: Pre-chemistry Avenue

The calculations described here are motivated by the observation that the active-site geometry of the closed structure of pol β resulting from our previous computational study [4, 10] differs from the idealized two-metal-ion geometry observed in the penta-covalent phosphoryl intermediate crystallized in 2003 [22].

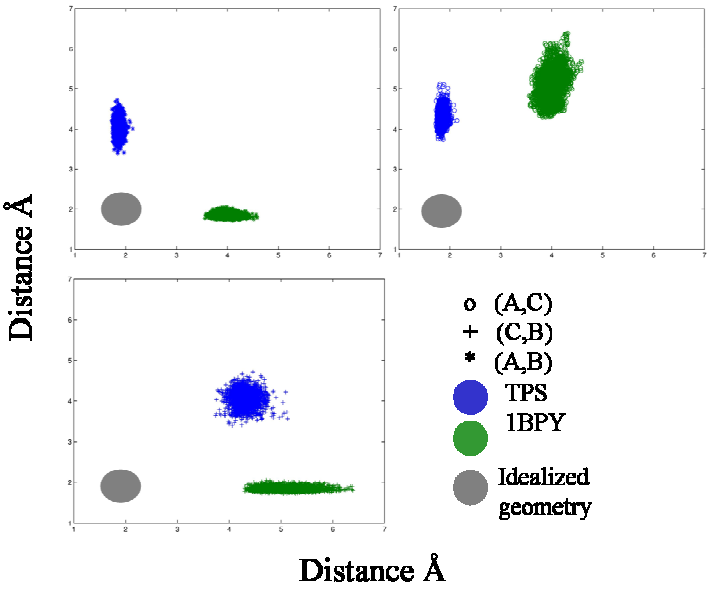

Figure S6: Comparison of key distances in the active site of pol β (**G:C**).

The range of values for distances A, B, and C observed in our closed model systems after transition path sampling is plotted as distance pairs. Here A, B, and C are the distances for $O1_{\alpha}$-dCTP─ Mg^{2+}(cat.), Mg^{2+}(cat.)─$O_{\delta 2}$ (Asp256), and Mg^{2+}(cat.)─O3′, respectively. The grey region in Figure S6 represents the ideal geometry for an associative or partially associative transition state [22]. The geometry of the closed structure resulting from our previous transition path sampling [6-8] simulations [4, 10] differs from the ideal geometry in that the distances B, C and D in the simulated structure (Fig. S6) are larger.

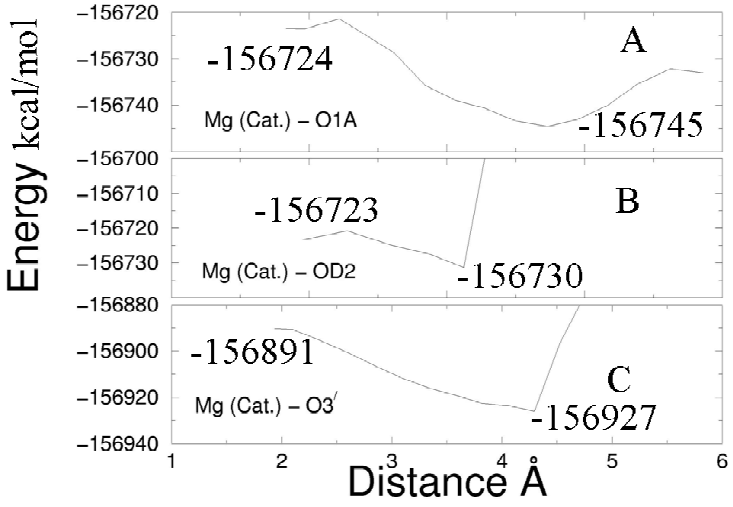

Figure S7: Energy profiles for **G:C** system of pol β.

Our current simulations are carried out for a fully solvated periodic system of pol β similar to those described in Ref. [4, 10]. With the objective of probing the energy landscape associated with the active site geometry and degrees of freedom, we performed constrained energy minimizations using the CHARMM program[23]. Constraints were applied one distance at a time along A, B, and C directions while leaving the other two unconstrained. The potential energy maps were constructed by plotting the energy for the different conformations explored in the constraint runs.

Pol β G:C system

The energy profiles obtained from constraint minimizations of the **G:C** system are reported in Figure S7. The energy landscape along B is relatively flat between 1.75 and 3.5 Å (variation of about 5 kcal/mol). The energy landscape along C indicates that constraining C to the ideal value in Figure S6 is associated with an energy cost of approximately 27 kcal/mol.

The path (in the 4-dimensional space of A, B, C, and D) traced by the resulting conformations of the constrained minimizations reveals an interesting feature (see Fig. S8). The almost vertical and horizontal traces in Figure S8 indicate that the "movement" along dimensions A, B and C are independent with little cross correlation, while the dimension D co-moves with C (the trace in Fig. S8 has a positive slope less than 90˚) and hence cannot be independently varied. Therefore, the 3-dimensional space of A, B and C provides independent and complete basis to describe the differences between the active site geometries of Figure S6, the 1BPY structure, and the closed structure resulting

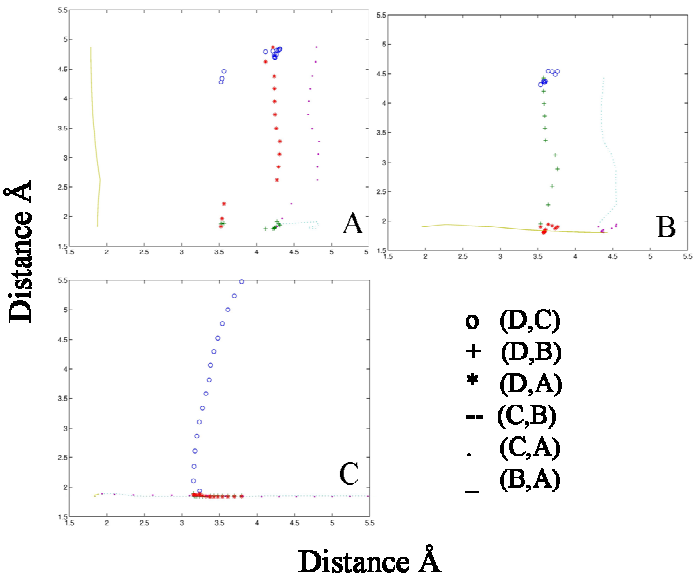

Figure S8: The co-movement of key active-site distances in the minimization runs. The labels (A, B, or C) represent the distance that was constrained. Each symbol corresponds to a specified pair of distances (see the legend key).

from TPS simulations.

Figures S6 and S7 show the different minima that exist close to the ideal geometry of Fig. 5 and their relative energies for the **G:C** system. In order to resemble the ideal geometry, the distances A, B and C have to fall within 2 Å, which automatically ensures that the distance D falls within the reactive distance (see Fig. S8). Figure S7 also shows that the ideal geometry has a relatively higher energy corresponding to other minima and hence can be envisioned to be the transition state. This definition of a transition state is consistent with the geometry of the penta-covalent phosphoryl intermediate found in Refs. [22, 24].

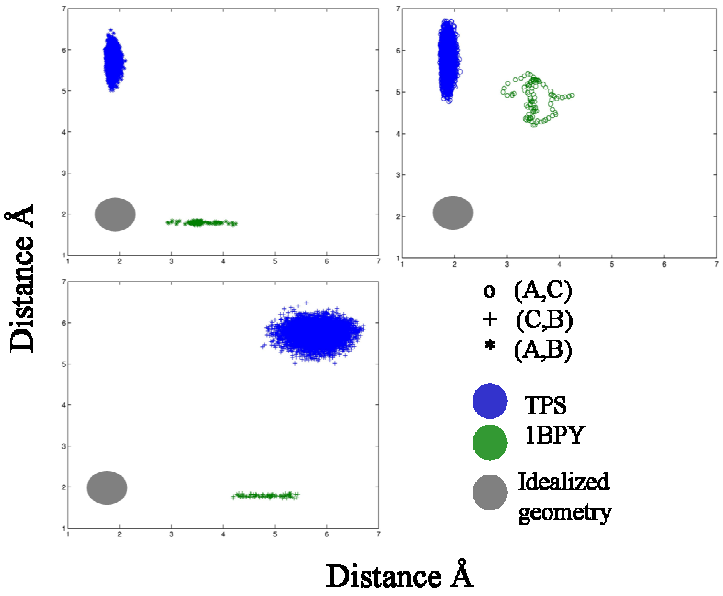

Figure S9: Comparison of key distances in the active site of pol β (**G:A**).

Pol β G:A system

The key distances A, B, C, and D for the **G:A** mispair system further deviate from the ideal geometry of Fig. 5 in comparison with the **G:C** matched case. These distances are shown in Fig. S9.

Similar to Figures S7 and S8 for the **G:C** system, the energy profiles and co-movement of key distances as obtained by constraint minimizations on the **G:A** system along A, B, and C directions are shown in Figures S10 and S11. For the **G:A** system, the energy landscape along A and B are relatively steep (variation of about 20 kcal/mol) indicating a much larger energy cost associated with transforming to the reactive (ideal) geometry.

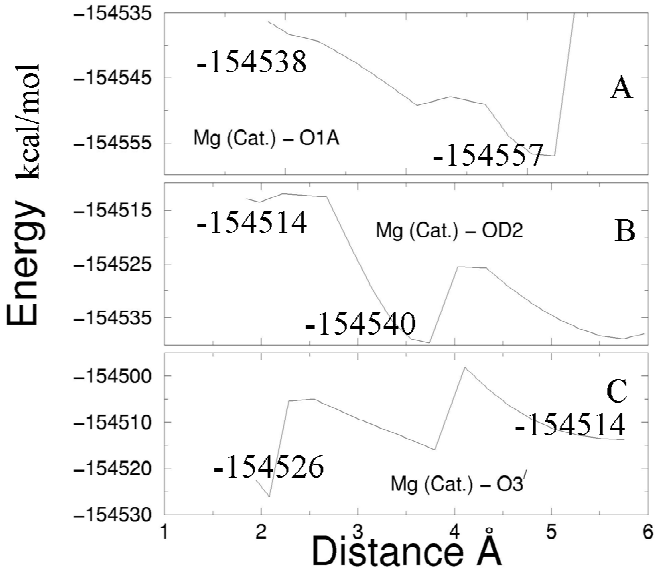

Figure S10: Energy profiles for **G:A** system.

The path (in the 4-dimensional space of A, B, C, and D) followed in the constrained minimization runs (Fig. S11) also reveals almost vertical and horizontal traces for pairs of distances not involving D. The traces also show cross correlations between D and C (like the **G:C** case) as well as D and A (unlike **G:C** case). Constraining A, B, and C to their ideal values does not reconstruct the "ideal" geometry in Fig. 5, as D is still far from 4 Å. Therefore, a trace was obtained by a series of minimizations in which D was constrained at several values and which resulted in a path different from the traces involving constraints along A, B, and C. This implies that unlike the **G:C** case, A, B, and C alone do not form a complete basis to transform the active-site geometry to the ideal one and the principal mode for this transformation involves D as well.

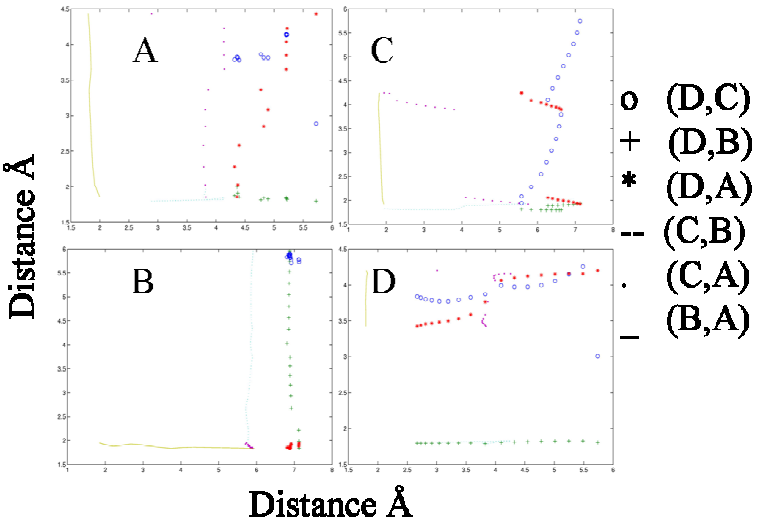

Figure S11: The co-movement of key active-site distances in the minimization runs for the **G:A** system. The labels (A, B, C, or D) represent the distance that was constrained. The symbols correspond to the trace of pairs of distances (see legend key).

Pre-Chemistry Avenue

The analysis of the energy landscapes (Fig. S12) associated with the active site degrees of freedom reveals that different minima exist close to but distinct from the ideal geometry. This suggests that, within the "closed conformation", the enzyme hops among localized molecular states of which only one (with A ≈ B ≈ C ≈ 2 Å) corresponds to the ideal geometry of the associative or partially-associative transition state. The relative probability of the system finding itself in this basin governs the rate of nucleotide incorporation (chemistry). The hopping between the different basins corresponds to subtle conformational changes in the active site involving the catalytic Mg^{2+} ion. The relatively high energy of the ideal configuration compared to the rest of the basins suggests that even from the closed

conformation, the nucleotide incorporation may be an activated process involving a large energy barrier. Another intriguing possibility is that pol β structure may have deliberately evolved to utilize these metastable basins in the "closed" conformation so as to introduce an additional check before carrying out the phosphoryl-transfer reaction. The fact that the active site geometry must undergo subtle conformational transitions within the closed state to reach the structure of the "ideal" transition state defines the pre-chemistry avenue for pol β.

The results for the solvated ternary complex of pol β/DNA/dATP with a **G:A** mispair suggest that the active site is further distorted from the ideal geometry, in comparison with the **G:C** matched pair. The energy profiles for **G:A** relative to **G:C** are steep (variation of about 20 kcal/mol) indicating a much larger energy cost associated with transforming the geometry to the ideal case. Furthermore, the cooperative motion in the active-site degrees of freedom appears to be different for the **G:A** system in comparison to the **G:C** case. For the correct **G:C** case, the reactive distance D is achieved via fluctuations in A, B, and C distances, while for the incorrect **G:A** case, the fluctuations in A, B, C are disengaged from D. This suggests a dynamic discrimination machinery of the pre-chemistry avenue, which likely provides an additional check before nucleotide incorporation. Our results for the energetics

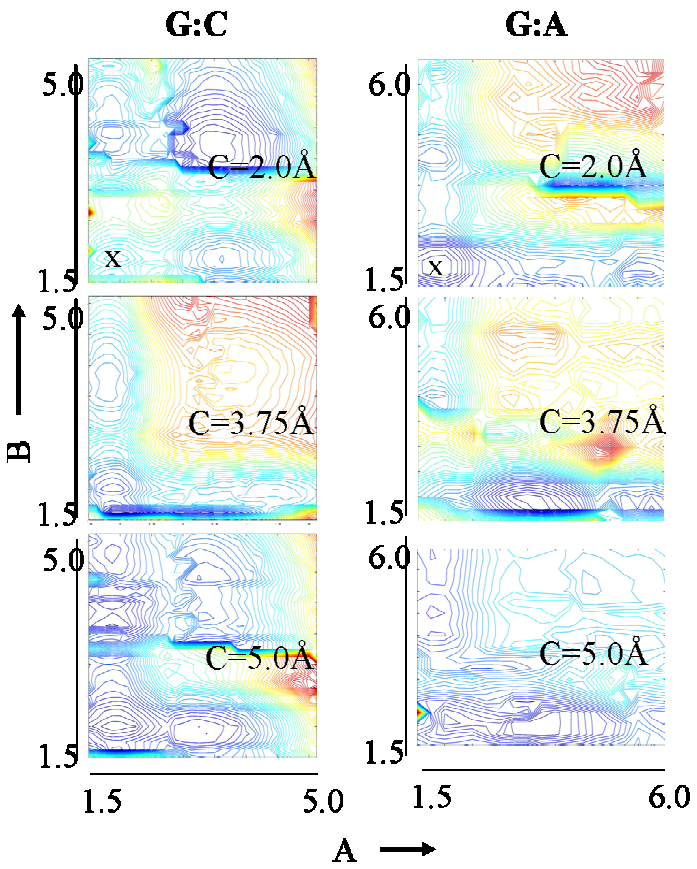

Figure S12: Comparison of the two-dimensional energy landscape. Potential energy, U(A,B) for the **G:C** and **G:A** systems of pol β for different slices along the distance C. The contours represent equal energy configurations (blue- local minima and red- local maxima). The energy valleys marked x correspond to the reactive (ideal two-metal-ion) geometry.

also indicate that the transition state is likely to have a much higher barrier for the **G:A** case, consistent with the reduced rate of **G:A** incorporation (by a factor of 1000) in comparison with **G:C**.

This evidence thus suggests that the evolutionary pressure can lead the enzyme to control the rate of phosphorylation by stabilizing the conformations at different values of the reaction coordinate distance (in comparison to the transition state), thereby driving the reaction through alternate mechanisms. Our hypothesis regarding the control of fidelity by altering the critical distance between the nucleophilic O3' oxyanion and the P_α of the incoming dNTP in the active site is consistent with the above notion.

Thus, all evidence points to subtle transformations of the active-site via the pre-chemistry avenue that provides additional checks and bounds before orchestrating the chemical reaction. In contrast to other well characterized polymerases, pol β is thought to regulate nucleotide incorporation [25] by a rate-limiting covalent incorporation step for correct as well as incorrect unit. The computational results point to a rich landscape associated with this step in the form of a pre-chemistry and chemistry (phosphoryl-transfer at the transition state).

Reference:

1. Arndt, J.W., et al., *Insight into the catalytic mechanism of DNA polymerase β: Structures of intermediate complexes.* Biochemistry, 2001. 40(18): p. 5368-5375.
2. Vande Berg, B.J., W.A. Beard, and S.H. Wilson, *DNA structure and aspartate 276 influence nucleotide binding to human DNA polymerase β - Implication for the identity of the rate-limiting conformational change.* J. Biol. Chem., 2001. 276(5): p. 3408-3416.
3. Yang, L.J., et al., *Polymerase β simulations suggest that Arg258 rotation is a slow step rather than large subdomain motions per se.* J. Mol. Biol., 2002. 317(5): p. 651-671.
4. Radhakrishnan, R. and T. Schlick, *Orchestration of cooperative events in DNA synthesis and repair mechanism unraveled by transition path sampling of DNA polymerase β's closing.* P. Natl. Acad. Sci. USA, 2004. 101(16): p. 5970-5975.
5. Arora, K. and T. Schlick, *In silico evidence for DNA polymerase-β's substrate-induced conformational change.* Biophys. J., 2004. 87(5): p. 3088-3099.
6. Bolhuis, P.G., C. Dellago, and D. Chandler, *Sampling ensembles of deterministic transition pathways.* Faraday Discussions, 1998(110): p. 421-436.
7. Bolhuis, P.G., et al., *Transition path sampling: Throwing ropes over rough mountain passes, in the dark.* Annual Review of Physical Chemistry, 2002. 53: p. 291-318.
8. Dellago, C., P.G. Bolhuis, and P.L. Geissler, *Transition path sampling*, in *Advances in Chemical Physics, Vol 123*. 2002. p. 1-78.
9. Radhakrishnan, R. and T. Schlick, *Biomolecular free energy profiles by a shooting/umbrella sampling protocol, "BOLAS"*. J. Chem. Phys., 2004. 121(5): p. 2436-2444.
10. Radhakrishnan, R. and T. Schlick, *Fidelity discrimination in DNA polymerase β: differing closing profiles for a mismatched G:A versus matched G:C basepair*. J. Am. Chem. Soc., 2005. 127: p. 13245-13252.

11. Sawaya, M.R., et al., *Crystal structures of human DNA polymerase β complexed with gapped and nicked DNA: Evidence for an induced fit mechanism.* Biochemistry, 1997. 36(37): p. 11205-11215.

12. Berg, B.J.V., W.A. Beard, and S.H. Wilson, *DNA structure and aspartate 276 influence nucleotide binding to human DNA polymerase β - Implication for the identity of the rate-limiting conformational change.* Journal of Biological Chemistry, 2001. 276(5): p. 3408-3416.

13. Menge, K.L., et al., *Structure-function analysis of the mammalian DNA polymerase β active site: Role of aspartic acid 256, arginine 254, and arginine 258 in nucleotidyl transfer.* Biochemistry, 1995. 34(49): p. 15934-15942.

14. Ahn, J.W., et al., *DNA polymerase β: effects of gapped DNA substrates on dNTP specificity, fidelity, processivity and conformational changes.* Biochemical Journal, 1998. 331: p. 79-87.

15. Ahn, J., B.G. Werneburg, and M.D. Tsai, *DNA polymerase β: Structure-fidelity relationship from pre-steady-state kinetic analyses of all possible correct and incorrect base pairs for wild type and R283A mutant.* Biochemistry, 1997. 36(5): p. 1100-1107.

16. Werneburg, B.G., et al., *DNA polymerase β: Pre-steady-state kinetic analysis and roles of arginine-283 in catalysis and fidelity.* Biochemistry, 1996. 35(22): p. 7041-7050.

17. Shah, A.M., et al., *Y265H mutator mutant of DNA polymerase β - Proper geometric alignment is critical for fidelity.* Journal of Biological Chemistry, 2001. 276(14): p. 10824-10831.

18. Beard, W.A., et al., *Enzyme-DNA interactions required for efficient nucleotide incorporation and discrimination in human DNA polymerase β.* Journal of Biological Chemistry, 1996. 271(21): p. 12141-12144.

19. Yang, L.J., et al., *Local deformations revealed by dynamics simulations of DNA polymerase β with DNA mismatches at the primer terminus.* J. Mol. Biol., 2002. 321(3): p. 459-478.

20. Yang, L.J., et al., *Critical role of magnesium ions in DNA polymerase β's closing and active site assembly.* J. Am. Chem. Soc., 2004. 126(27): p. 8441-8453.

21. Yang, L.J., et al., *Highly organized but pliant active site of DNA polymerase β: Compensatory mechanisms in mutant enzymes revealed by dynamics simulations and energy analyses.* Biophys. J., 2004. 86(6): p. 3392-3408.

22. Lahiri, S.D., et al., *The pentacovalent phosphorus intermediate of a phosphoryl transfer reaction.* Science, 2003. 299(5615): p. 2067-2071.

23. Brooks, B.R., et al., *Charmm - a program for macromolecular energy, minimization, and dynamics calculations.* J. Comput. Chem., 1983. 4(2): p. 187-217.

24. Stahley, M.R. and S.A. Strobel, *Structural evidence for a two-metal-ion mechanism of group I intron splicing.* Science, 2005. 309(5740): p. 1587-1590.

25. Joyce, C.M. and S.J. Benkovic, *DNA polymerase fidelity: Kinetics, structure, and checkpoints.* Biochemistry, 2004. 43(45): p. 14317-14324.